Journal of
Synchrotron Radiation

ISSN 0909-0495

Received 25 March 2011
Accepted 4 July 2011

Quantum critical point in $SmO_{1-x}F_xFeAs$ and oxygen vacancy induced by high fluorine dopant

Jie Cheng,[a,b] Shengqi Chu,[b] Wangsheng Chu,[a,b]* Wei Xu,[b] Jing Zhou,[b] Linjuan Zhang,[b] Haifeng Zhao,[b] Ronghua Liu,[c] Xianhui Chen,[c] Augusto Marcelli[d,e] and Ziyu Wu[a,b]*

[a]National Synchrotron Radiation Laboratory, University of Science and Technology of China, Hefei, Anhui 230029, People's Republic of China, [b]Beijing Synchrotron Radiation Facility, Institute of High Energy Physics, Chinese Academy of Sciences, Beijing 100049, People's Republic of China, [c]Hefei National Laboratory for Physical Science at Microscale and Deparment of Physics, University of Science and Technology of China, Hefei 230026, People's Republic of China, [d]Istituto Nazionale di Fisica Nucleare, Laboratori Nazionali di Frascati, 00044 Frascati, Italy, and [e]University of Science and Technology of China, Chinese Academy of Science, Hefei 230026, People's Republic of China. E-mail: cws@ihep.ac.cn, wuzy@ustc.edu.cn

The local lattice and electronic structure of the high-T_c superconductor $SmO_{1-x}F_xFeAs$ as a function of F-doping have been investigated by Sm L_3-edge X-ray absorption near-edge structure and multiple-scattering calculations. Experiments performed at the L_3-edge show that the white line (WL) is very sensitive to F-doping. In the under-doped region ($x \leq 0.12$) the WL intensity increases with doping and then it suddenly starts decreasing at $x = 0.15$. Meanwhile, the trend of the WL linewidth *versus* F-doping levels is just contrary to that of the intensity. The phenomenon is almost coincident with the quantum critical point occurring in $SmO_{1-x}F_xFeAs$ at $x \simeq 0.14$. In the under-doped region the increase of the intensity is related to the localization of Sm-*5d* states, while theoretical calculations show that both the decreasing intensity and the consequent broadening of linewidth at high F-doping are associated with the content and distribution of oxygen vacancies.

Keywords: $SmO_{1-x}F_xFeAs$; XANES; oxygen vacancy.

1. Introduction

The recent discovery of iron-based superconductors (Chen, Wu *et al.*, 2008; Kamihara *et al.*, 2008; Takahashi *et al.*, 2008) whose transition temperature has been raised up to 56 K has once again triggered research on high-T_c superconductors (Chen, Tesanovic *et al.*, 2008; Chiao, 2008; Grant, 2008), just as happened after the 1986 discovery of copper-based superconductors (Bednorz & Müller, 1986; Wu *et al.*, 1987). Similar to cuprates, iron-based superconductors have quasi-two-dimensional structure, and an FeAs layer which is separated by ReO (Re = La, Sm *etc.*) or R (R = Ba, Sr *etc.*) charge reservoir layers has been considered as the superconductive layer, like the CuO_2 layer in cuprates. The majority of the studies have focused on the properties of the FeAs layers (Shimojima *et al.*, 2010; Zhang *et al.*, 2010); however, charge reservoir layers are equally important for characterizing these high-T_c superconductors. As an example, the local geometry out of the Cu—O plane in cuprate superconductors dramatically affects T_c (Fujita *et al.*, 2005; Gao *et al.*, 2009). Recent research performed on iron-based $ReFeAsO_{1-x}F_x$ systems (Chen, Wu *et al.*, 2008; Kamihara *et al.*, 2008) showed large variations of T_c when changing the rare-earth (Re) ion. Therefore, a more accurate characterization of ReO layers may be useful to better understand the superconductive properties of iron-based superconductors.

Synchrotron-radiation-based X-ray absorption near-edge structure (XANES) is a well recognized local experimental technique capable of investigating the short/medium-range order and the electronic structure of a material (Bianconi *et al.*, 1982; Chu *et al.*, 2009; Wu *et al.*, 1996). Re L_3-edge XANES was applied to study Re-containing compounds (Centeno *et al.*, 2000; Espeso *et al.*, 2000) such as cuprate superconductors (Tan *et al.*, 1990; Wu *et al.*, 1998). Recently, it has also been used to explore the valence electronic structure and the local geometry of the ReO slab of iron-based superconductors (Joseph *et al.*, 2009; Xu *et al.*, 2010). Still there is a lack of a systematic analysis of the relationship between doping concentration and structural characteristics of ReO layers.

In this contribution we have focused on the $SmO_{1-x}F_xFeAs$ system (Chen, Wu *et al.*, 2008), which was the first iron-based superconductor compound that exceeded the McMillan limit within the framework of the Bardeen–Cooper–Schrieffer theory (Bardeen *et al.*, 1957). The resistivity of its parent

compound SmOFeAs exhibits a clear anomaly, and the Hall coefficient sharply increases at $T_s \simeq 148$ K, pointing out the onset of a structural transition (Liu *et al.*, 2008). With F-doping, T_s decreases, and superconductivity emerges at $x \simeq 0.07$ (Liu *et al.*, 2008). The Sm L_3-edge XANES spectra show that the Sm—O bond length is independent of F-doping although it affects the medium-range shell around Sm atoms. Moreover, while the white line (WL) intensity *versus* F-doping first increases, it then abruptly decreases owing to oxygen vacancies induced by high F-doping.

2. Experiments and calculations

Polycrystalline $SmO_{1-x}F_xFeAs$ compounds (x = 0, 0.05, 0.12, 0.15, 0.18) were synthesized by conventional solid-state reaction method (Liu *et al.*, 2008). It should be pointed out that at high doping levels, say $x > 0.12$, a tiny amount of impurity phases like SmAs and SmOF is observed (Liu *et al.*, 2008; Yang *et al.*, 2009). Samples were ground into fine powders and then brushed onto tapes. Sm L_3-edge XANES spectra were collected at room temperature in transmission mode at the 1W1B beamline of the Beijing Synchrotron Radiation Facility. The storage ring was working at an electron energy of 2.5 GeV with a maximum stored current of about 250 mA. Data were collected using a Si (111) double-crystal monochromator and normalized using the *IFEFFIT* program (Newville, 2001).

Theoretical Sm L_3-edge XANES spectra were simulated in the framework of the multiple-scattering (MS) theory (Lee & Pendry, 1975; Natoli *et al.*, 1990) using the *FEFF8.2* code (Ankudinov *et al.*, 1998) within the muffin-tin approximation. The cluster for the simulations was generated using the *ATOMS* package (Ravel, 2001) using the *P*4/*nmm* space group with lattice constants a = 3.932 Å and c = 8.490 Å. The Hedin–Lundqvist exchange-correlation potential (Natoli *et al.*, 1990; Tyson *et al.*, 1992) was chosen in the calculations. A cluster of 55 atoms was applied in all MS calculations to obtain an accurate self-consistent field, and the full MS calculation converges using a cluster up to 14 shells (about 6 Å).

3. Results and discussions

Fig. 1(*a*) shows the normalized Sm L_3-edge XANES spectra of the $SmO_{1-x}F_xFeAs$ samples. As expected, all spectra are characterized by similar features: an intense WL feature *A*, a weak structure *B* followed by two strong resonance peaks (labelled as *C*1 and *C*2, respectively). It is well known that L_3-edge XANES is dominated by dipole-allowed transitions from *p* initial states to final unoccupied states of *d* and *s* character. Since the $p \rightarrow d$ transition is much stronger than $p \rightarrow s$, the latter could be neglected for describing the L_3-edge. We have to underline also that the single peak of the WL feature is different from that of the CeO_2 (Soldatov *et al.*, 1994) or some other mixed-valent Re-containing materials (Lübcke *et al.*, 1986; Singhal *et al.*, 1990). Actually the $SmO_{1-x}F_xFeAs$ system does not show a valence change *versus* F-doping. Regarding the weak peak *B*, recently Xu *et al.* (2010) pointed out that it is related to MS contributions originating from the geometrically

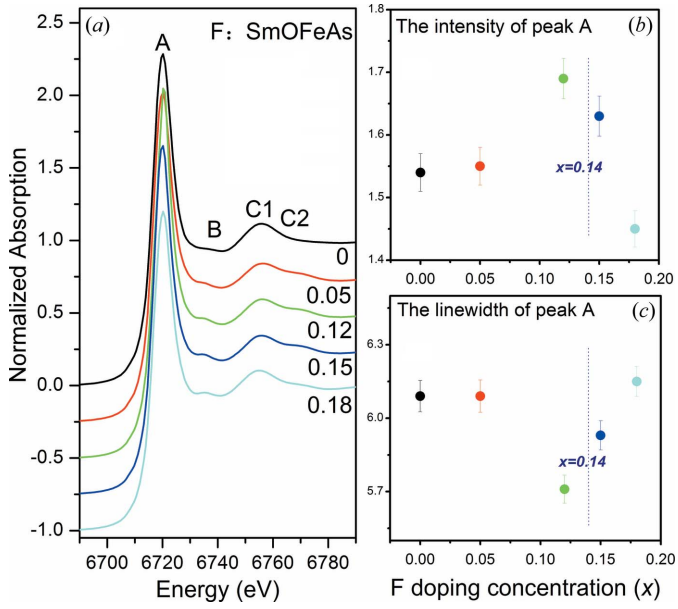

Figure 1
(*a*) Normalized Sm L_3-edge XANES spectra of $SmO_{1-x}F_xFeAs$ (x = 0, 0.05, 0.12, 0.15, 0.18) samples. (*b*) Plot of the WL intensity *versus* F-doping. (*c*) Plot of the WL linewidth *versus* F-doping. The dotted line indicates the F-concentration of the QCP (x = 0.14) in $SmO_{1-x}F_xFeAs$. The error bars represent the finite experimental errors in the estimation of the WL intensity and linewidth.

symmetric oxygen and iron positions. Finally, the resonance features *C*1 and *C*2 have been empirically associated with MS contributions involving the nearest neighbours of As and O atoms (Joseph *et al.*, 2009).

In order to identify the origin of the latter resonance peaks, we performed systematic MS XANES calculations at the Sm L_3-edge by using different clusters. In Fig. 2 we show the atomic structure around the Sm absorber while in Fig. 3(*a*) we compare different calculations. For a minimal cluster of five atoms, containing the central Sm atom surrounded only by

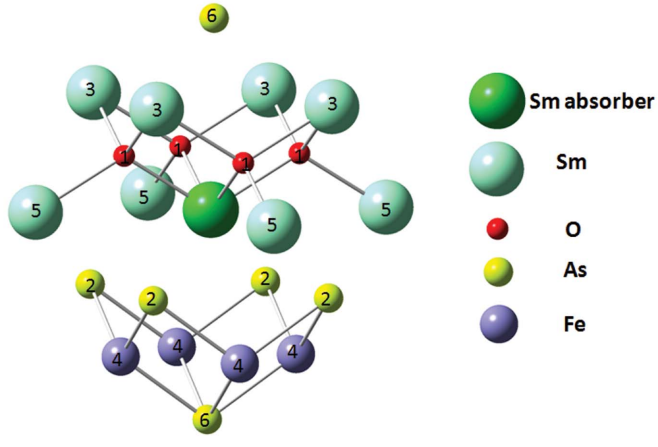

Figure 2
The representative atomic cluster around a central Sm absorber. Coloured spheres are Sm (cyan online), O (red), As (yellow) and Fe (purple). In order to see the coordination environment clearly, the Sm absorber is marked in green. Numbers identify atoms belonging to different shells around the Sm absorber.

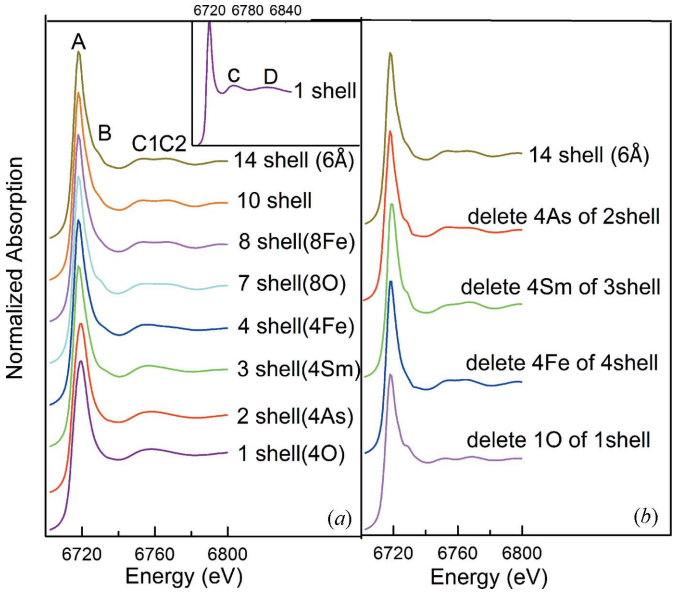

Figure 3
(*a*) MS XANES calculations at the Sm L_3-edge as a function of the cluster size. (*b*) Sm L_3-edge XANES spectra obtained with different cluster models.

the first shell containing four O atoms (see Fig. 2), only the WL peak *A* and the features *C* and *D* appear [see the inset in Fig. 3(*a*)]. Therefore, the resonance peaks *C* and *D* are due to multiple- and single-scattering contributions, respectively, within the first oxygen coordination shell in the real space. Only after adding the fourth shell to this atomic cluster does the feature *C*2 appear, although it is not separated by *C*1. It clearly sharpens, increasing the cluster size up to the tenth shell, pointing out the relevance of the medium-range order in this system. To gain further insight into the role of MS to the feature *C*2 within the fourth shell, we carried out other tests shown in Fig. 3(*b*). By looking at both the *C*2 intensity and the intensity ratio *C*1/*C*2, we also found a correlation among the nearest O atoms and Sm atoms in the third shell that clearly contribute to the *C*2 structure. As a consequence both short- and medium-range order affect the peak *C*2.

Based on the above calculations, Sm L_3-edge XANES may be used to characterize the effect of F-doping on the local lattice and on the electronic structure. Fig. 1(*a*) clearly shows that both the position and the intensity of *C*1 are constant while *C*2 changes slightly with F-doping. Data pointed out that the Sm—O bond is rigid but the medium-range order may be still sensitive to perturbations. Moreover, by increasing the F-content the feature *B* becomes more defined; a mechanism that can be associated with an increase of disorder of O atoms (Xu *et al.*, 2010). More important is the significant change of the WL intensity and linewidth *versus* F-doping shown in Figs. 1(*b*) and 1(*c*). It should be noted that the Sm L_3-edge XANES were fit based on the least-squares method using one arctangent step function representing the transition to the continuum and several absorption peaks such as peak *A*, *B* *etc.*, and then we can obtain the intensity and linewidth of peak *A*. The intense WL feature at the absorption threshold corresponds to the atomic-like $2p \rightarrow 5d$ transition. Its changes are mainly driven by the characters of 5*d*-unoccupied states, *e.g.* localization or hybridization properties (Espeso *et al.*, 2000). In the under-doped region ($x \leq 0.12$) the WL intensity increases with doping, followed by a reduction of the linewidth. Because the Sm valence state remains constant, the significant increase of the WL intensity and the reduction of the linewidth can be only attributed to an increase of localization of the Sm-5*d* states, in agreement with a similar mechanism observed in the F-doped NdOFeAs (Joseph *et al.*, 2009). However, at $x = 0.15$, the intensity drops and then it further decreases at $x = 0.18$. Meanwhile, as shown in Fig. 1(*c*), the linewidth of the WL broadens at high F-doping levels. This sudden turnaround of the WL intensity/linewidth between under-doped and high F-doping regions almost coincides with the quantum critical point (QCP) of the $SmO_{1-x}F_xFeAs$-based system at $x \simeq 0.14$. At the QCP we observed: (i) a drastically different temperature dependence of the resistivity on both sides of the doping value $x \simeq 0.14$ (Liu *et al.*, 2008); (ii) a sharp change of the pressure coefficient $d(\ln T_c)/dP$ turning from positive to negative (Takabayashi *et al.*, 2008); (iii) a crossover from the orthorhombic ($x < 0.14$) to the tetragonal ($x > 0.14$) symmetry for the superconducting phase, *i.e.* a complete suppression of the structural transition at $x \simeq 0.14$ (Margadonna *et al.*, 2009). Although direct correlation of XANES WL and QCP remains unclear, the coincidence of the abrupt change of WL intensity/linewidth and the QCP observed using other techniques implies interesting physics played by the QCP on both local lattice and electronic structure, and also on the superconductive mechanism.

In order to rule out the influence of impurity phases at high doping levels ($x > 0.12$) on our discussion, we performed MS calculations of Sm L_3-edge XANES for potential impurities, SmAs and SmOF phases. The simulated spectra are shown in Fig. 4. One can easily exclude the effect of SmAs owing to its strikingly different XANES features from that of $SmFeAsO_{1-x}F_x$. As for the impurity SmOF, its spectrum features look almost identical to those of our doped samples, but the features *B* and *C* of SmOF are not at the correct positions (about 5 eV deviation from that of $x = 0.15$). Provided a large amount of impurity phases, the experimental XANES would show detectable and distinct features coming from the impurity phase. Referring to the experiment features of our doped sample up to $x = 0.18$, the obvious change is about the WL. Thus it is reasonable to conclude that the minor impurity phases impose negligible effect on our experimental XANES, which mainly indicates the inherent characteristic of the majority phase, thus rationalizing our discussion about the WL intensity/linewidth *versus* F-doping.

A careful electron microprobe analysis (EMPA) showed that in high F-doped $NdO_{1-x}F_xFeAs$ samples the complete occupancy of oxygen and fluorine sites is less than 1, pointing out the existence of oxygen vacancies (Malavasi *et al.*, 2010). Moreover, it was shown that F atoms cannot be doped in SmFeAsO without oxygen vacancies (Yang *et al.*, 2009). To interpret the variation of the WL intensity, we propose a conceptual scenario involving the oxygen vacancy existing

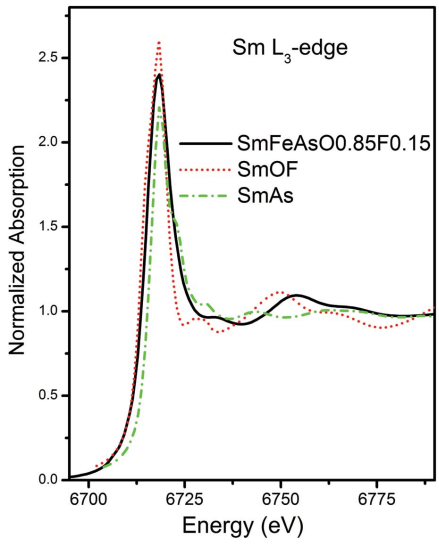

Figure 4
Comparison between the experimental Sm L_3-edge XANES spectrum of $SmFeAsO_{0.85}F_{0.15}$ and theoretical spectra of the SmOF and SmAs impurity phases.

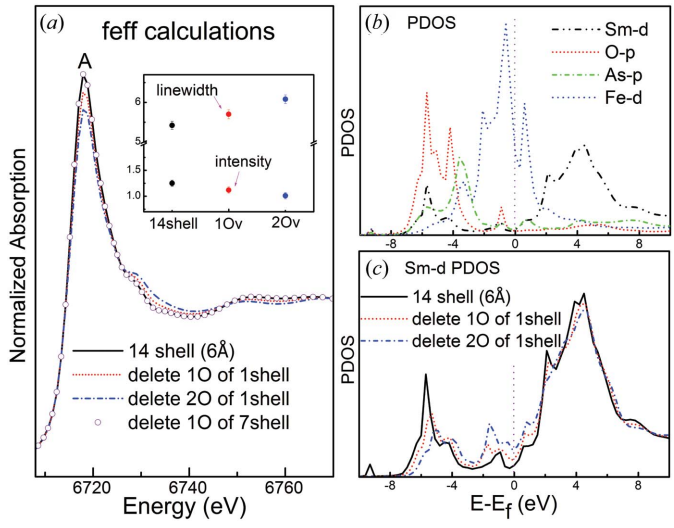

Figure 5
(*a*) MS XANES calculations at the Sm L_3-edge *versus* the oxygen vacancy in different shells. The inset shows both the intensity and linewidth of peak *A* as a function of oxygen vacancies in the first shell. (*b*) PDOS of each atomic species of SmOFeAs. (*c*) PDOS of the Sm-*d* state *versus* oxygen vacancy in the first shell. The Fermi level is set to 0 eV.

throughout the doping levels and the localization of Sm-*d* states as mentioned (Joseph *et al.*, 2009). It is the competition between oxygen vacancy and localization of Sm-*d* states that gives rise to the variation of WL. In the under-doped regime, the reduction effect imposed by oxygen vacancy on WL intensity is quite smaller than the enhancement effect by localization of Sm-*d* states; consequently the WL intensity increases with doping levels. By contrast, at higher doping levels, the WL intensity decreases because the effects of oxygen vacancies are predominant over that of localization of Sm-*d* states. To justify the scenario, we calculated both XANES spectra and the projected density of state (PDOS) with different vacancy configurations.

Four O atoms compose the first shell around the central Sm absorber, and eight form the seventh shell. We carried out MS XANES calculations at the Sm L_3-edge with different oxygen vacancy distributions in the first or seventh shell. Simulations summarized in Fig. 5(*a*) show that oxygen vacancies in the first shell may lead to a reduction of the WL intensity and an obvious broadening of the WL linewidth, while almost no changes are detectable for the lack of an O atom in the seventh shell. As a consequence, both the reduction intensity and the broadening linewidth of the WL can be correlated only to the oxygen vacancy in the first shell around the Sm ion.

Looking at the structure of the $SmO_{1-x}F_xFeAs$-based system, FeAs and SmO/F alternating layers are connected by Sm—As bonds (Chen, Wu *et al.*, 2008) and superconductivity emerges *via* electron transfer from SmO/F to FeAs layers. To better understand the role of oxygen vacancy on the electronic structure, PDOS calculations shown in Figs. 5(*b*) and 5(*c*) were also performed. Similar to the LaOFeP system (Lebegue, 2007), in Fig. 5(*b*) the Sm and As PDOS of the SmOFeAs share common structures around −7 to +8 eV, which leads to a hybridization interaction between these two atoms. Fig. 5(*c*) points out that the Sm-*d* PDOS at the Fermi level increases with the oxygen vacancy, the peak at −5.5 eV moves towards the −4 eV structure of the As atom, while the structure around 4.4 eV widens and decreases in intensity. The changes of the Sm-*d* PDOS induced by the oxygen vacancy may enhance the hybridization between Sm and As atoms, promote the interlayer electron transfer and possibly be the superconductive mechanism.

4. Conclusion

We have analyzed Sm L_3-edge XANES spectra using accurate MS calculations to investigate the F-doping mechanism and its influence on the lattice and electronic structure of the high-T_c superconducting system $SmO_{1-x}F_xFeAs$. XANES shows two resonance features *C*1 and *C*2 (see Fig. 1*a*) that detailed MS calculations assigned to contributions from nearest O atoms (*C*1) and to short/medium-range contributions (*C*2). The analysis demonstrates that the F-doping may finely tune the short/medium-range order around the Sm atoms. On the other hand, data show that the WL intensity *versus* doping does not increase monotonically but abruptly decreases at a high F-doping level, in agreement with the occurrence of a QCP in the $SmO_{1-x}F_xFeAs$ system. Further MS and PDOS calculations point out that this reduction of the intensity and the consequent broadening of WL linewidth may be associated with the oxygen vacancy distribution. Moreover, the presence of an oxygen vacancy in the first shell enhances the hybridization between Sm and As atoms and this mechanism may be certainly beneficial to the superconductivity.

This work was partly supported by the National Outstanding Youth Fund (Project No. 10125523 to ZW) and by the Knowledge Innovation Program of the Chinese Academy of Sciences (KJCX2-YW-N42). Furthermore, WSC

thanks the National Science Foundation of China (No. 10805055) and the innovation fund of the Institute of High Energy Physics (IHEP) for young researchers (No. 542009IHEPZZBS50845).

References

Ankudinov, A. L., Ravel, B., Rehr, J. J. & Conradson, S. D. (1998). *Phys. Rev. B*, **58**, 7565–7576.

Bardeen, J., Cooper, L. N. & Schrieffer, J. R. (1957). *Phys. Rev.* **108**, 1175–1204.

Bednorz, J. G. & Müller, K. A. (1986). *Z. Phys.* **64**, 189–193.

Bianconi, A., Dell'Ariccia, M., Durham, P. J. & Pendry, J. B. (1982). *Phys. Rev. B*, **26**, 6502–6508.

Centeno, M. A., Malet, P., Carrizosa, I. & Odriozola, J. A. (2000). *J. Phys. Chem. B*, **104**, 3310–3319.

Chen, T. Y., Tesanovic, Z., Liu, R. H., Chen, X. H. & Chien, C. L. (2008). *Nature (London)*, **453**, 1224–1227.

Chen, X. H., Wu, T., Wu, G., Liu, R. H., Chen, H. & Fang, D. F. (2008). *Nature (London)*, **453**, 761–762.

Chiao, M. (2008). *Nat. Phys.* **4**, 446.

Chu, W. S., Marcelli, A., Hu, T. D., Wei, S. Q., Liu, W. H., Saini, N. L., Bianconi, A. & Wu, Z. Y. (2009). *New J. Phys.* **11**, 083005.

Espeso, J. I., Gómez Sal, J. C. & Chaboy, J. (2000). *Phys. Rev. B*, **63**, 014416.

Fujita, K., Noda, T., Kojima, K. M., Eisaki, H. & Uchida, S. (2005). *Phys. Rev. Lett.* **95**, 097006.

Gao, W. B., Liu, Q. Q., Yang, L. X., Yu, Y., Li, F. Y., Jin, C. Q. & Uchida, S. (2009). *Phys. Rev. B*, **80**, 094523.

Grant, P. M. (2008). *Nature (London)*, **453**, 1000–1001.

Joseph, B., Iadecola, A., Fratini, M., Bianconi, A., Marcelli, A. & Saini, N. L. (2009). *J. Phys. Condens. Matter*, **21**, 432201.

Kamihara, Y., Watanabe, T., Hirano, M. & Hosono, H. (2008). *J. Am. Chem. Soc.* **130**, 3296–3297.

Lebegue, S. (2007). *Phys. Rev. B*, **75**, 035110.

Lee, P. A. & Pendry, J. B. (1975). *Phys. Rev. B*, **11**, 2795.

Liu, R. H., Wu, G., Wu, T., Fang, D. F., Chen, H., Li, S. Y., Liu, K., Xie, Y. L., Wang, X. F., Yang, R. L., Ding, L., He, C., Feng, D. L. & Chen, X. H. (2008). *Phys. Rev. Lett.* **101**, 087001.

Lübcke, M., Sonntag, B., Niemann, W. & Rabe, P. (1986). *Phys. Rev. B*, **34**, 5184.

Malavasi, L., Artioli, G. A., Ritter, C., Mozzati, M. C., Maroni, B., Pahari, B. & Caneschi, A. (2010). *J. Am. Chem. Soc.* **132**, 2417–2420.

Margadonna, S., Takabayashi, Y., McDonald, M. T., Brunelli, M., Wu, G., Liu, R. H., Chen, X. H. & Prassides, K. (2009). *Phys. Rev. B*, **79**, 014503.

Natoli, C. R., Benfatto, M., Brouder, C., López, M. F. R. & Foulis, D. L. (1990). *Phys. Rev. B*, **42**, 1944.

Newville, M. (2001). *J. Synchrotron Rad.* **8**, 322–324.

Ravel, B. (2001). *J. Synchrotron Rad.* **8**, 314–316.

Shimojima, T., Ishizaka, K., Ishida, Y., Katayama, N., Ohgushi, K., Kiss, T., Okawa, M., Togashi, T., Wang, X. Y., Chen, C. T., Watanabe, S., Kadota, R., Oguchi, T., Chainani, A. & Shin, S. (2010). *Phys. Rev. Lett.* **104**, 057002.

Singhal, R. K., Rao, K. V. R., Chandra, U., Garg, K. B., Jain, D. C. & Beeken, R. B. (1990). *Phys. Scr.* **41**, 284–288.

Soldatov, A. V., Ivanchenko, T. S., Della Longa, S., Kotani, A., Iwamoto, Y. & Bianconi, A. (1994). *Phys. Rev. B*, **50**, 5074.

Takabayashi, Y., McDonald, M. T., Papanikolaou, D., Margadonna, S., Wu, G., Liu, R. H., Chen, X. H. & Prassides, K. (2008). *J. Am. Chem. Soc.* **130**, 9242–9243.

Takahashi, H., Igawa, K., Arii, K., Kamihara, Y., Hirano, M. & Hosono, H. (2008). *Nature (London)*, **453**, 376–378.

Tan, Z., Filipkowski, M. E., Budnick, J. I., Heller, E. K., Brewe, D. L., Chamberland, B. L., Bouldin, C. E., Woicik, J. C. & Shi, D. (1990). *Phys. Rev. Lett.* **64**, 2715–2718.

Tyson, T. A., Hodgson, K. O., Natoli, C. R. & Benfatto, M. (1992). *Phys. Rev. B*, **46**, 5997.

Wu, M. K., Ashburn, J. R., Torng, C. J., Hor, P. H., Meng, R. L., Gao, L., Huang, Z. J., Wang, Y. Q. & Chu, C. W. (1987). *Phys. Rev. Lett.* **58**, 908–910.

Wu, Z. Y., Benfatto, M. & Natoli, C. R. (1998). *Phys. Rev. B*, **57**, 10336.

Wu, Z. Y., Ouvrard, G., Lemaux, S., Moreau, P., Gressier, P., Lemoigno, F. & Rouxel, J. (1996). *Phys. Rev. Lett.* **77**, 2101–2104.

Xu, W., Marcelli, A., Joseph, B., Iadecola, A., Chu, W. S., Di Gioacchino, D., Bianconi, A., Wu, Z. Y. & Saini, N. L. (2010). *J. Phys. Condens. Matter*, **22**, 125701.

Yang, J., Ren, Z. A., Che, G. C., Lu, W., Shen, X. L., Li, Z. C., Yi, W., Dong, X. L., Sun, L. L., Zhou, F. & Zhao, Z. X. (2009). *Supercond. Sci. Technol.* **22**, 025004.

Zhang, C. J., Oyanagi, H., Sun, Z. H., Kamihara, Y. & Hosono, H. (2010). *Phys. Rev. B*, **81**, 094516.